Supporting Information

Graphene Aerogels that Withstand Extreme Compressive Stress and Strain

Chenwei Li,[a,b,c,] Meichun Ding,[d] Baoqing Zhang,[a,b] Xin Qiao,[a] and Chen-Yang Liu[a,b,]**

a. CAS Key Laboratory of Engineering Plastics, CAS Research/Education Center for Excellence in Molecular Sciences, Institute of Chemistry, the Chinese Academy of Sciences, Beijing 100190, China.
E-mail: lichenwei@iccas.ac.cn; liucy@iccas.ac.cn

b. University of Chinese Academy of Sciences, Beijing 100049, China

c. College of Materials Science and Engineering, Institute for Graphene Applied Technology Innovation, Qingdao University, Qingdao 266071, China.

d. College of Chemistry and Molecular Engineering, State Key Laboratory Base of Eco-Chemical Engineering, Qingdao University of Science and Technology, Qingdao 266042, China.

Contents

Movie S1: Compression test (90% strain) of t-GA-500 by Rheometer (20 N)

Movie S2: Compression test (90% strain) of GA by Rheometer (20 N)

Movie S3: Compression test (＞99% strain) of t-GA-500 by Universal Tensile Machine (5000 N)

Tables and Figures

Characterization of Graphene Oxide

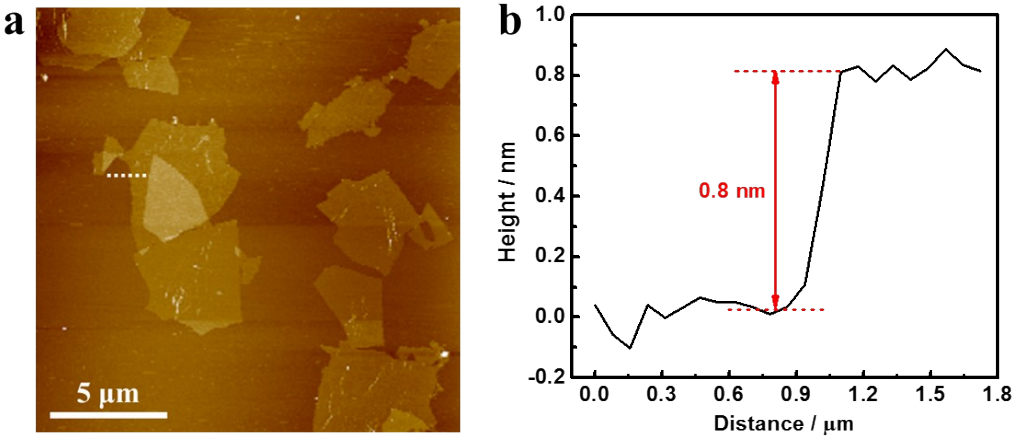

Figure S1. Atomic force microscopy (AFM) image (a) and its corresponding height profile (the dotted line) (b) show that the graphene oxide (GO) sheets are monolayer (~ 0.8 nm thick) with the average size less than 5 µm.

Images of t-GA-500 with Different Shapes

Figure S2. Digital images of t-GA-500 with different shapes.

SEM Images of GA and t-GA-500

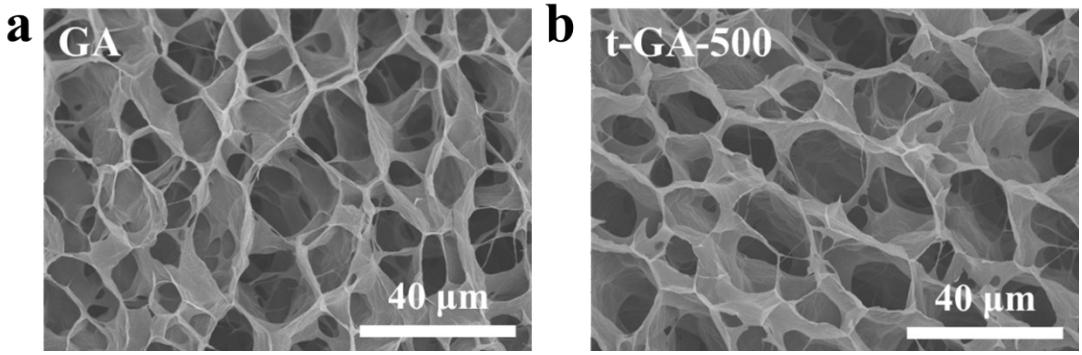

Figure S3. SEM images of GA (a) and t-GA-500 (b) at high magnification.

The Ratios of the Density of GA after annealing at 500 °C to that of GA

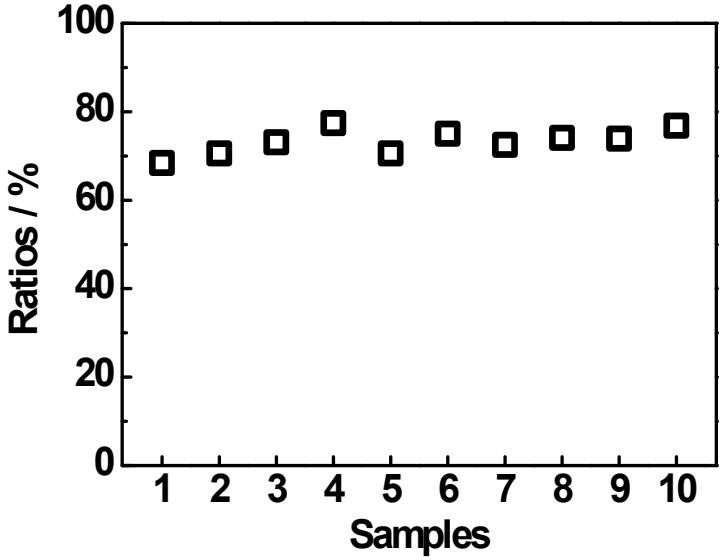

Figure S4. The ratios of the density of t-GA-500 to that of GA. It can be seen that after thermal-treatment, the density of t-GA-500 decreased by about 30 percent. The densities of t-GA-500 and GA are obtained from the data shown in Figure 1f.

The Densities of GA and t-GA-500 as a Function of GO Concentration

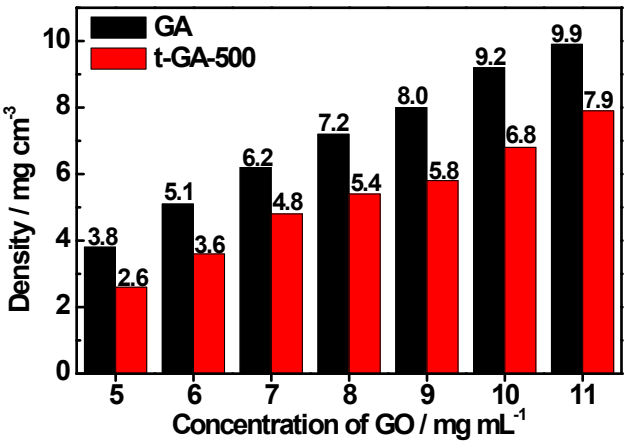

Figure S5. The densities of GA and t-GA-500 as a function of GO concentration.

Cyclic Compressive Tests of t-GA-500 with the Increasing Strains

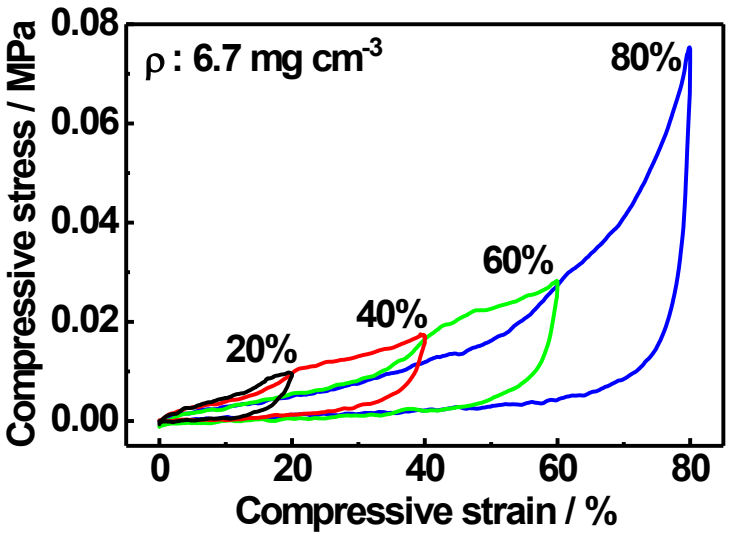

Figure S6. The stress-strain curve of t-GA-500 (6.7 mg cm^{-3}) at different compressive strains. Compared to stress-strain curve with 20% strain, the slope of stress-strain curve with 40% strain decreased slightly, indicating that slight damage of the graphene network structures during compression at 20% strain.

Compressive Stress-Strain Curves of GA with the Strain of 90%

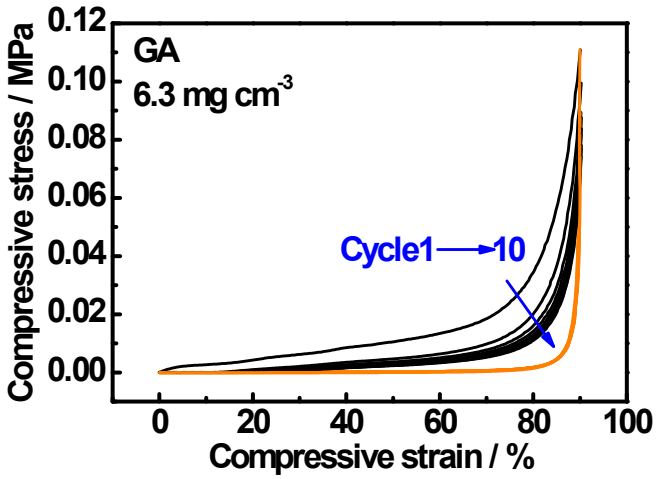

Figure S7. Compressive stress-strain curves of GA of 10 cycles of loading (black lines) and unloading (orange lines) with the maximum strain of 90%.

Physical Properties of t-GA-500 with Different Densities

Table S1. Physical properties of t-GA-500 with different densities in the first compression cycle. The compression tests was performed using the ARES-G2 with a 20 N force sensor.

Density [mg cm^{-3}]	Young's modulus [MPa]	Compressive strength at 80% strain [MPa]	Compressive strength at 90% strain [MPa]
4.1	0.022	0.025	0.038
4.5	0.032	0.028	0.064
5.0	0.032	0.035	0.096
5.8	0.048	0.042	0.117
6.0	0.057	0.042	0.125
6.3	0.050	0.047	0.129
6.8	0.083	0.059	0.157
7.0	0.062	0.054	0.145
7.4	0.071	0.061	0.178
7.5	0.093	0.073	0.180
7.9	0.094	0.072	0.190

The Dependence of Compressive Stress and Young's Modulus on Density

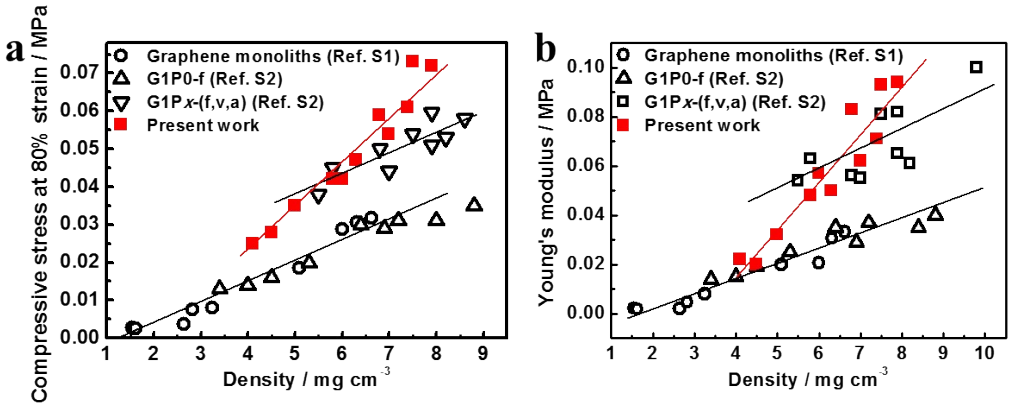

Figure S8. The mechanical properties of t-GA-500 in this work compared with other graphene-based aerogels: (a) comparison of the ultimate compressive stress at 80% strains, (b) comparison of the Young's modulus.

Compressive Stress-strain Curves of t-GA-500 at Different Compress/release Rates

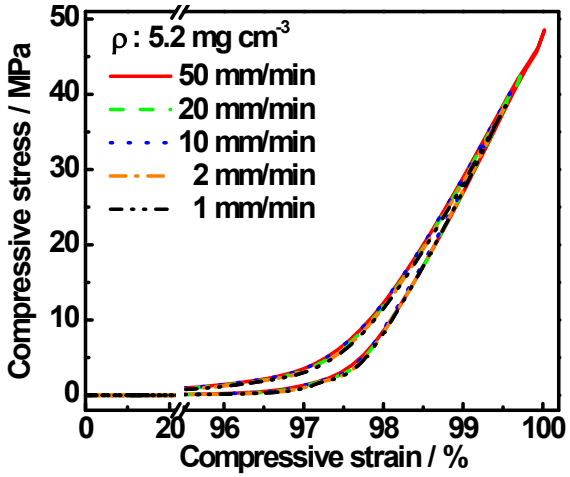

Figure S9. The stress-strain curves of t-GA-500 at different compress/release rates. The crossover in the stress-strain curves when the strain exceeded 99% was induced by fast compressive rates (50 mm/min) and grow bigger with the increasing of compressive rates.

SEM and HRTEM Images of t-GA-500 with Different Densities

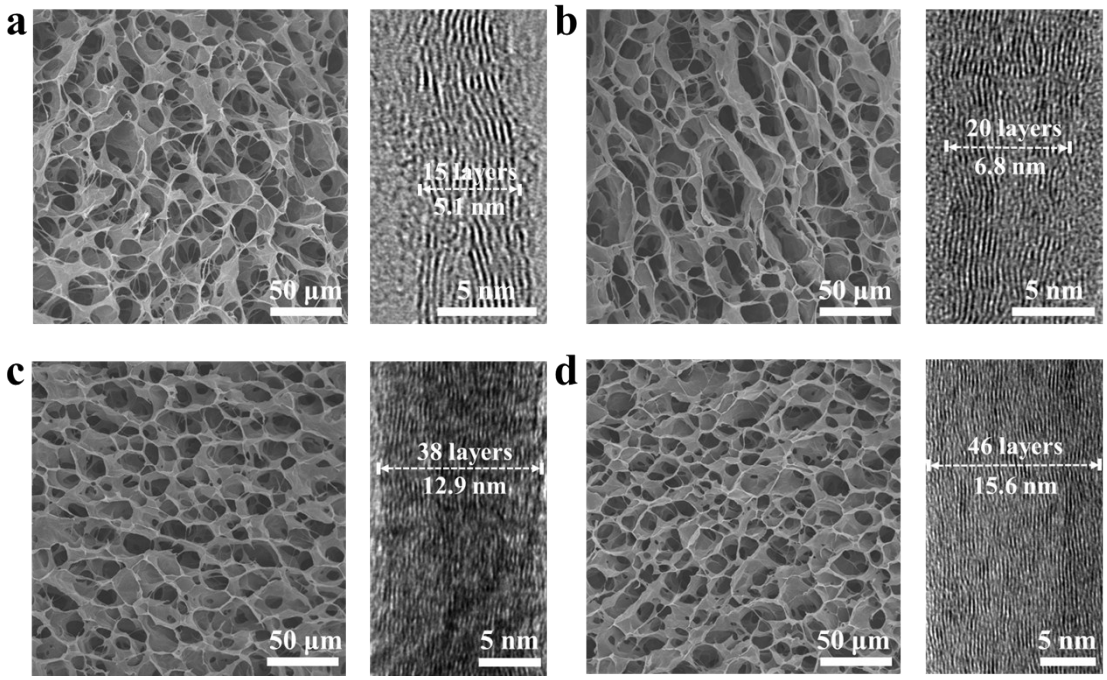

Figure S10. SEM (left) and HRTEM (right) images of t-GA-500 with a density of ~2 (a), ~4 (b), ~6 (c) and ~8 mg cm^3 (d). The thinkness of cell wall of t-GA-500 was directly measured by using HRTEM technique. And the number of graphene layers obtain from HRTEM images are consistent with the values which are the thinkness of cell wall divided by the average d-spacing obtained from the XRD spectra (Figure 1e). T-GA-500 with the density of ~2 mg cm^3 had thinner cell walls (~15 layers) which were composed of lesser graphene sheets than those of t-GA-500 (the cell walls composed of above 20 layers) with high density (4~8 mg cm^3). Therefore, the network structures of the t-GA-500 (~2 mg cm^3) were easily broken due to thinner cell walls during severe compression.

The SEM Images of GA after the Ultimate Compression (100,000 N, 60 min)

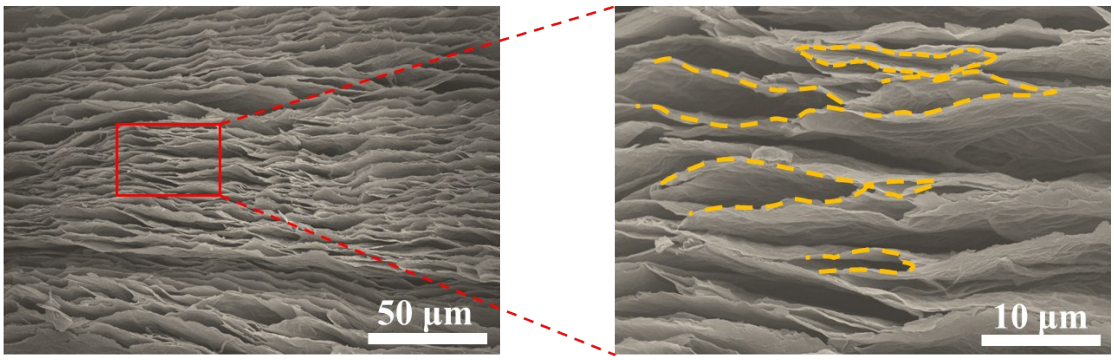

Figure S11. SEM images of GA after the ultimate compression (100,000 N, 60 min) and the selected area (red square) was enlarged.

The SEM Images of t-GA-500 after the Ultimate Compression (100,000 N, 60 min)

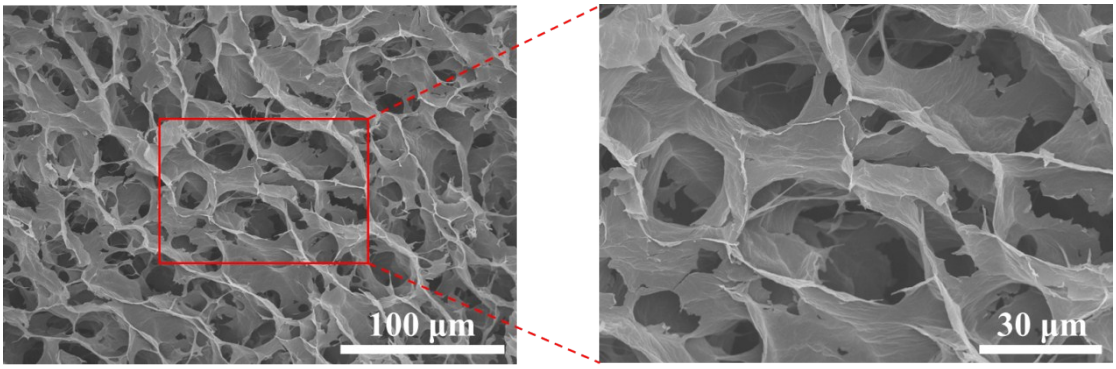

Figure S12. SEM images of t-GA-500 after the ultimate compression (100,000 N, 60 min) and the selected area (red square) was enlarged.

Schematic Illustration of the t-GA-500 and Lead-Tin Alloy during the Compress/release Cycle

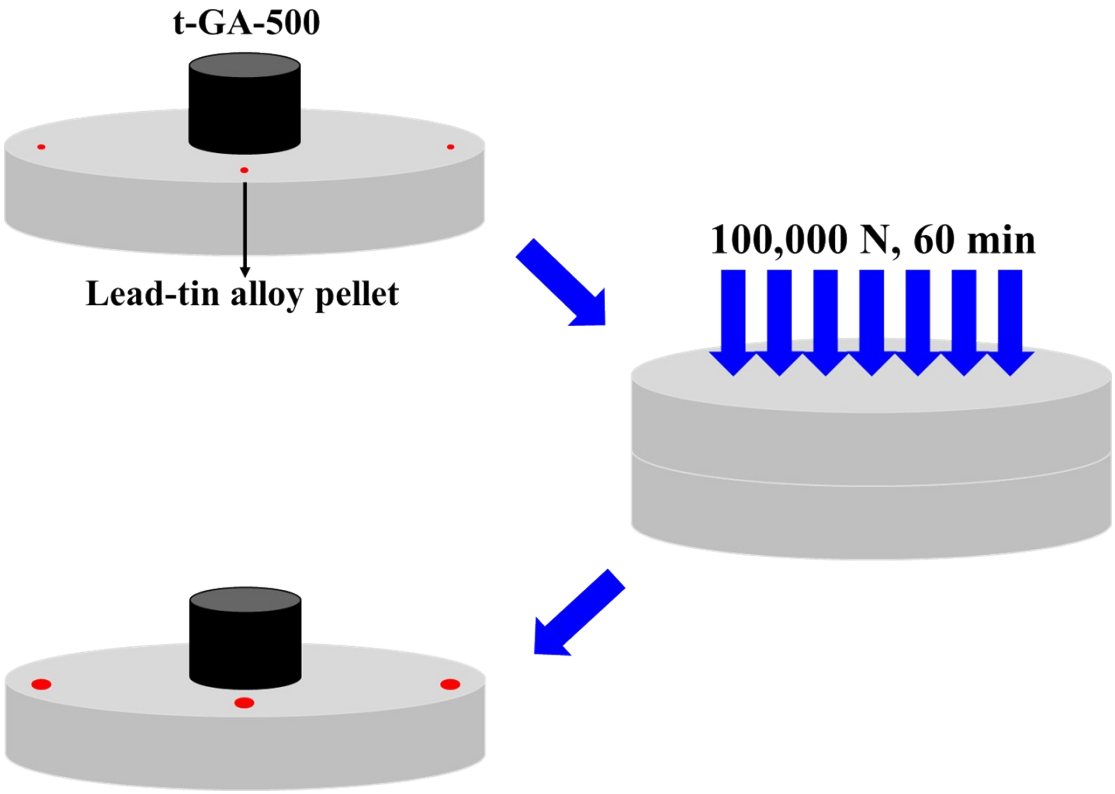

Figure S13. The illustration of the t-GA-500 and lead-tin alloy deformation during the ultimate compress/release cycle. The thickness of t-GA-500 under 100,000 N was measured according to the average thickness of lead-tin alloy foils.

The Thickness and Maximum Strain of t-GA-500 during the Extreme Compression

Table S2. The thickness and maximum strain of t-GA-500 during the extreme compression (100,000 N, 60 min).

Sample	Density [mg cm^{-3}]	Height [mm]	Thickness [a)] [mm]	Maximum strain [%]
t-GA-500	7.4	11.08	0.035	99.7
t-GA-500	5.8	11.68	0.025	99.8
t-GA-500	6.0	11.72	0.037	99.7
t-GA-500	5.8	12.80	0.023	99.8
t-GA-500	4.5	12.04	0.024	99.8
t-GA-500	4.5	11.85	0.022	99.8

[a)] The thickness of t-GA-500 during the extreme compression (100,000 N for 60 min) was measured by the average thickness of three lead-tin alloy foils.

Physical Properties of t-GA-500 Compared with Other Superelastic Graphene Aerogels

Table S3. Compressive properties of other reported superelastic graphene aerogels, the maximum strain, maximum stress, and the maximum stress normalized by density.

Sample	Density [mg cm^{-3}]	Maximum strain [%]	Ultimate stress [MPa]	Ultimate stress / Density [MPa / mg cm^{-3}]	Ref
Graphene monolith	5.1	80	0.019	0.004	S1
G1P1-f	5.8	80	0.044	0.008	S2
Nanocarbon aerogel complexes	~5	80	0.003	0.001	S3
RF–GO–metal compressible aerogel	31.2	80	0.09	0.003	S4
Carbonaceous nanofibers aerogel	21.34	80	0.078	0.004	S5
rGO-porous network	11	80	~0.13	0.012	S6
Graphene-coated nanotube aerogel	14	80	~0.3	0.020	S7
Graphene aerogels	~16	90	0.017	0.001	S8
Ultralight graphene aerogels (ULGAs)	~3	90	0.02	0.007	S9
C-G Monolith	13.8	90	0.105	0.008	S10
Graphene / CNTs hybird foams	~8	90	~0.072	0.009	S11
Fe3O4/graphene aerogels	5.8	95	0.01	0.002	S12
Graphene aerogels	10	95	0.028	0.003	S13
3D graphene	3.3	95	~3	0.909	S14
Graphene sponge	~1	98	0.085	0.085	S15
Graphene Metamaterial	8	99	0.7	0.088	S16
NDGA	9.25	99	1.5	0.162	S17
SGF-0.3	25.45	99	5.4	0.212	S18
t-GA-500 [a)]	7.6	99.0	31.16	4.10	This work
t-GA-500 [a)]	6.3	99.2	32.89	5.22	This work
t-GA-500 [a)]	5.4	99.5	39.96	7.40	This work
t-GA-500 [a,b)]	6.8	99.6	57.12	8.40	This work
t-GA-500 [a)]	5.2	99.6	36.76	7.07	This work
t-GA-500 [a)]	4.3	99.7	35.91	8.35	This work
t-GA-500 [c)]	7.4	99.7 [d)]	725	98	This work
t-GA-500 [c)]	5.8	99.8 [d)]	647	112	This work
t-GA-500 [b,c)]	6.0	99.7 [d)]	1047	174	This work
t-GA-500 [b,c)]	5.8	99.8 [d)]	1057	182	This work
t-GA-500 [c)]	4.5	99.8 [d)]	609	135	This work

t-GA-500 [c)]	4.5	99.8 [d)]	649	144	This work

[a)]The compression test for t-GA-500 was carried out under the maximum weight of 5000 N.
[b)] t-GAs cube samples (height: 1.0~1.5 cm, side length: ~1.0 cm).
[c)]The compression test for t-GA-500 was carried out under the maximum weight of 100,000 N.
[d)]The thickness of t-GA-500 during the extreme compression (100,000 N for 60 min) was measured by the average thickness of lead-tin alloy foils (The specific illustration was shown in Figure S12).

Physical Properties of t-GA-500 Compared with Other Elastic Porous Materials

Table S4. Compressive properties of other reported elastic porous materials, the maximum strain, maximum stress, and the maximum stress normalized by density.

Sample	Density [mg cm^{-3}]	Maximum strain [%]	Ultimate stress [MPa]	Ultimate stress / Density [MPa / mg cm^{-3}]	Ref
Silsesquioxane aerogel	64	56	0.038	0.0006	S19
Silsesquioxane aerogel	74	65	0.162	0.0021	S19
Silsesquioxane aerogel	85	62	0.212	0.0025	S19
SiO_2 aerogel	1.5	80	0.00135	0.0009	S20
SiO_2 aerogel	5.0	80	0.00433	0.0009	S20
Ternary silicone sponge	104.7	80	0.145	0.0014	S21
Ni foam	14	50	0.0111	0.0008	S22
Ni foam	43	50	0.143	0.0033	S22
Ni-P foam	10.2	50	0.109	0.0107	S23
Al foam	12	50	1.2	0.1	S24
PVA/Cellulose nanofibril aerogel	16	85	0.24	0.015	S25
Chitosan aerogel	20	50	0.044	0.0022	S26
Bacterial cellulose aerogel	6.69	95	0.125	0.0187	S27
Bacterial cellulose aerogel	6.77	95	0.138	0.0204	S27
Bacterial cellulose aerogel	6.75	95	0.152	0.0225	S27
Epoxy/graphene oxide (97/3) aerogel	90	99.2	0.021	0.0002	S28
Epoxy/graphene oxide (95/5) aerogel	89	99.5	0.065	0.0007	S28
Epoxy/graphene oxide (93/7) aerogel	93	99.6	0.148	0.0016	S28
Epoxy/graphene oxide (91/9) aerogel	92	99.6	0.231	0.0025	S28
PAA(20%)/graphene aerogel	5.3	80	0.034	0.00657	S29
PAA(30%)/graphene aerogel	6.4	80	0.041	0.00641	S29
PAA(50%)/graphene aerogel	6.7	80	0.058	0.00867	S20
Graphene-wrapped melamine sponge	10	75	0.030	0.003	S30
Polyurethane/graphene aerogel	24.6	80	0.145	0.0059	S31
CNT sponge	11.88	80	0.115	0.0097	S32
Aerogel with sacrificial template of PU	4.8	50	0.002	0.00042	S33
Aerogel with sacrificial template of melamine foam	3.3	95	0.134	0.041	S34
Aerogel with sacrificial template of melamine foam	4.5	95	0.192	0.043	S34
Aerogel with sacrificial template of melamine foam	6.1	95	0.324	0.053	S34

Aerogel with sacrificial template of melamine foam	7.4	94	0.54	0.073	S34
Aerogel with sacrificial template of PU	8.8	80	0.00004	0.000005	S35
Aerogel with sacrificial template of melamine foam	16.3	90	0.7	0.043	S36
Aerogel with sacrificial template of Ni foam	5.5	40	0.000013	0.0000024	S37
t-GA-500 [a)]	7.6	99.0	31.16	4.10	This work
t-GA-500 [a)]	6.3	99.2	32.89	5.22	This work
t-GA-500 [a)]	5.4	99.5	39.96	7.40	This work
t-GA-500 [a,b)]	6.8	99.6	57.12	8.40	This work
t-GA-500 [a)]	5.2	99.6	36.76	7.07	This work
t-GA-500 [a)]	4.3	99.7	35.91	8.35	This work
t-GA-500 [c)]	7.4	99.7 [d)]	725	98	This work
t-GA-500 [c)]	5.8	99.8 [d)]	647	112	This work
t-GA-500 [b,c)]	6.0	99.7 [d)]	1047	174	This work
t-GA-500 [b,c)]	5.8	99.8 [d)]	1057	182	This work
t-GA-500 [c)]	4.5	99.8 [d)]	609	135	This work
t-GA-500 [c)]	4.5	99.8 [d)]	649	144	This work

[a)]The compression test for t-GA-500 was carried out under the maximum weight of 5000 N.
[b)] t-GAs cube samples (height: 1.0~1.5 cm, side length: ~1.0 cm).
[c)]The compression test for t-GA-500 was carried out under the maximum weight of 100,000 N.
[d)]The thickness of t-GA-500 during the extreme compression (100,000 N for 60 min) was measured by the average thickness of lead-tin alloy foils (The specific illustration was shown in Figure S12).

TGA Curves of GA Annealed at Different Temperature

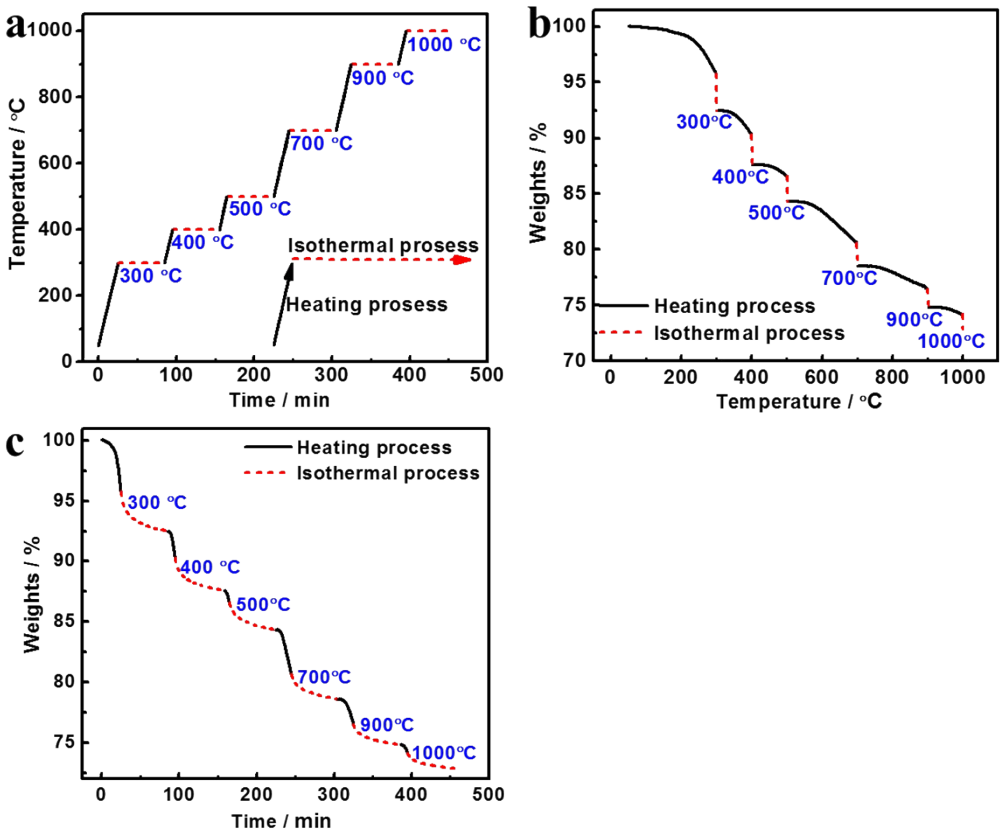

Figure S14. TGA curves of GA in a nitrogen atmosphere. (a) The heating and isothermal programming. GA was heated from 50 to 1000 °C at a heating rate of 10 °C min^{-1} under a N_2 atmosphere and annealed at 300, 400, 500, 700, 900, and 1000 °C for 1 h, respectively; (b) TGA curves of GA changed with temperature; (c) TGA curves of GA changed with time.

The Densities of GA and t-GA-(300~1000)

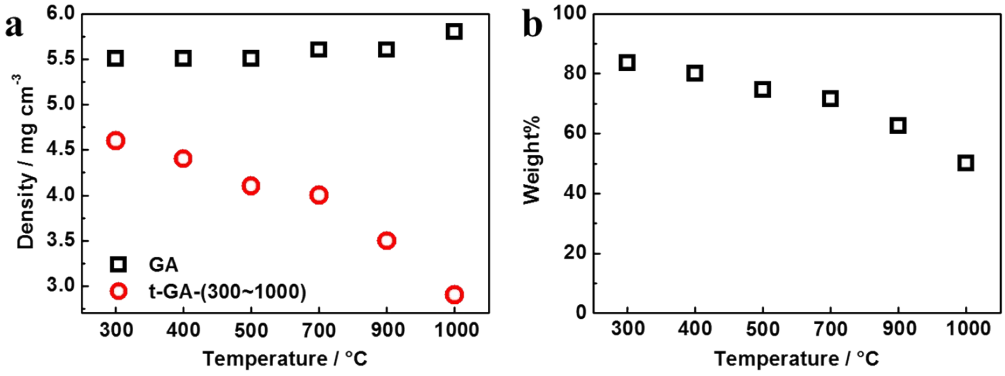

Figure S15. (a) The densities of GA before and after the annealing at 300~1000 °C; (b) The ratios of density of GA after the annealing at 300~1000 °C to that of GA. The ratios were calculated by the density of GA after the annealing at 300~1000 °C devided to that of GA in the Figure (a).

Compressive Stress-strain Curves of t-GA-(300,400,700,900,1000) with the Strain of 90%

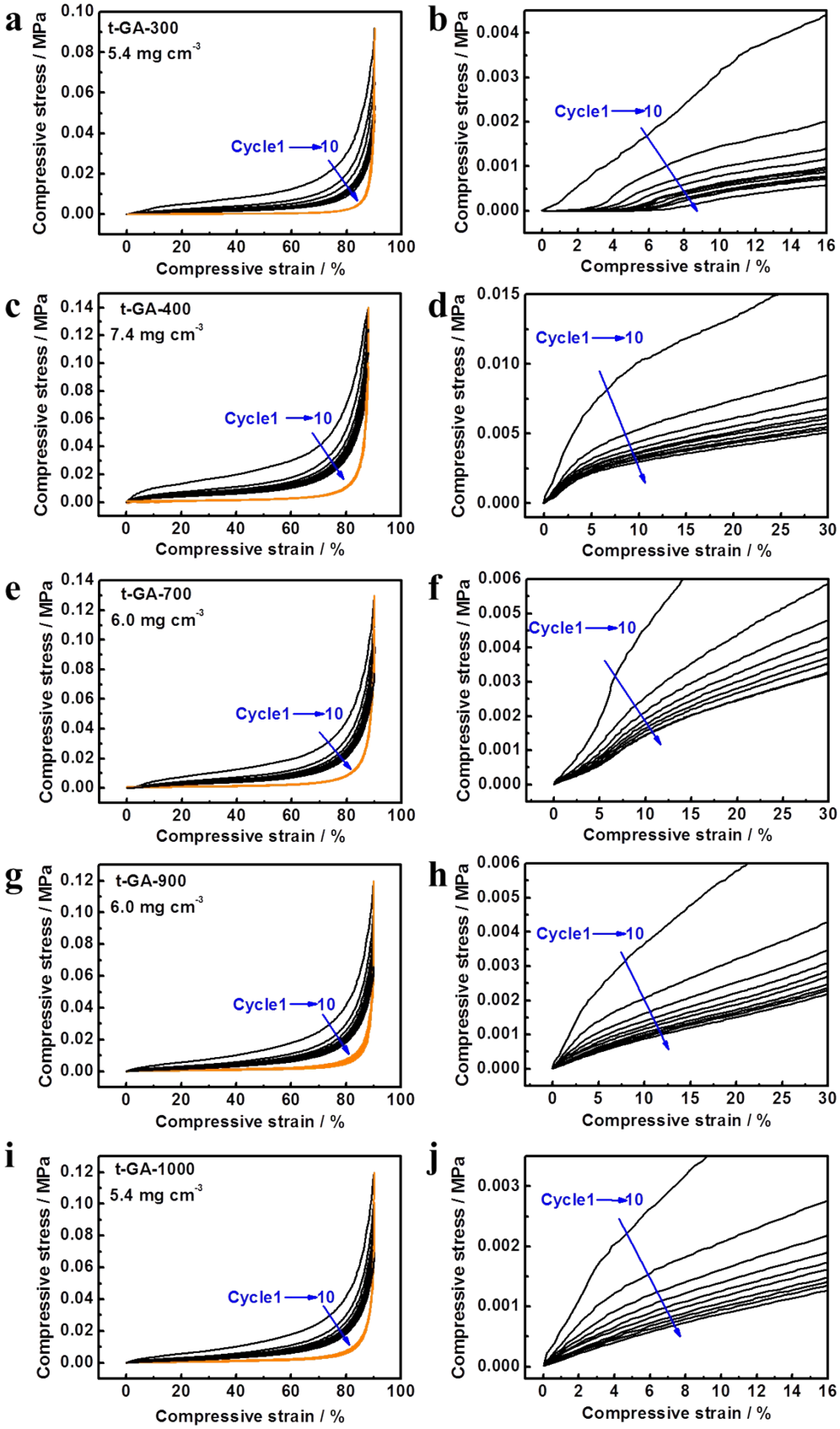

Figure S16. Compressive stress-strain curves of 10 cycles of loading (black lines) and unloading (orange lines): (a) t-GA-300; (b) t-GA-300 (the enlarged image at low stress area);

(c) t-GA-400; (d) t-GA-400 (the enlarged image at low stress area); (e) t-GA-700; (f) t-GA-700 (the enlarged image at low stress area); (g) t-GA-900; (h) t-GA-900 (the enlarged image at low stress area); (i) t-GA-1000; (j) t-GA-1000 (the enlarged image at low stress area).

XPS Analysis of GA and t-GA-(300~1000)

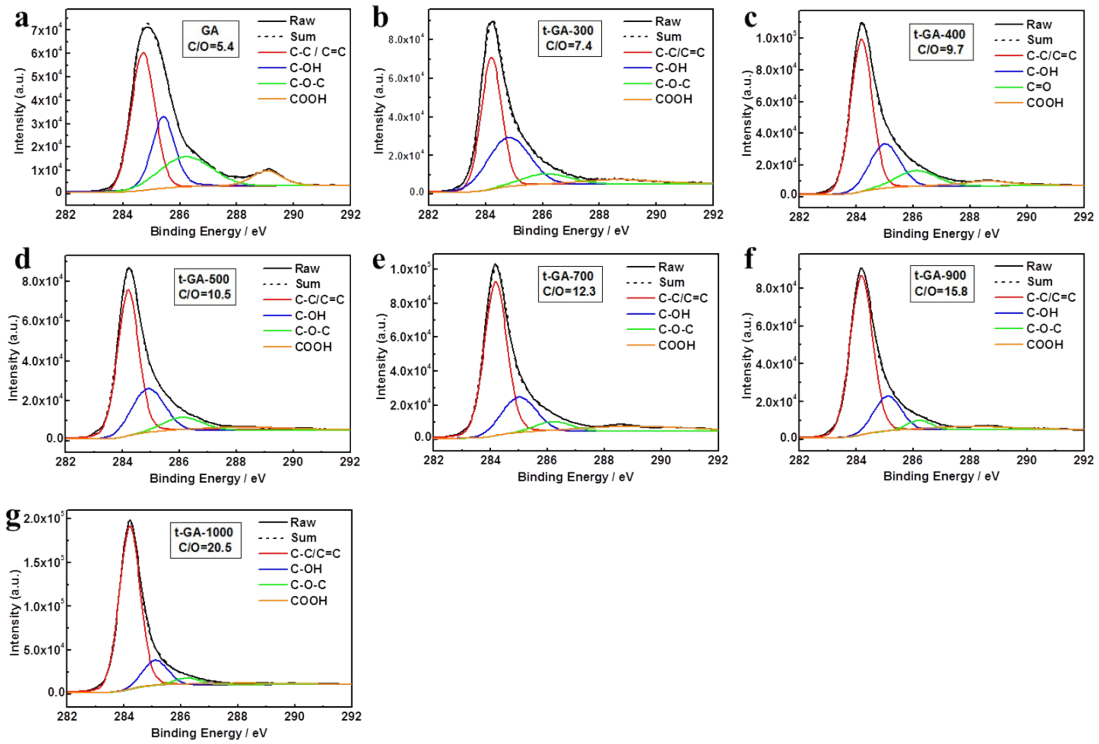

Figure S17. XPS spectra for C1s of the GA (a), t-GA-300 (b), t-GA-400 (c), t-GA-500 (d), t-GA-700 (e), t-GA-900 (f), and t-GA-1000 (g). Inset: the C/O mole ratio.

Elemental Analysis of GA and t-GA-(300~1000)

Table S5. Elemental analysis results of GA and t-GA-(300~1000). The data of element type and content come from XPS analysis (Figure S16).

Sample	C (wt%)	O (wt%)	N (wt%)	C/O (atomic ratio)
GA	84.79	15.56	0.65	5.38
t-GA-300	87.68	11.85	0.47	7.40
t-GA-400	90.21	9.28	0.51	9.72
t-GA-500	90.69	8.63	0.68	10.51
t-GA-700	92.19	7.48	0.33	12.32
t-GA-900	93.65	5.94	0.41	15.76
t-GA-1000	94.98	4.64	0.38	20.47

N_2 Adsorption-desorption Isotherms of GA and t-GA-(300~1000)

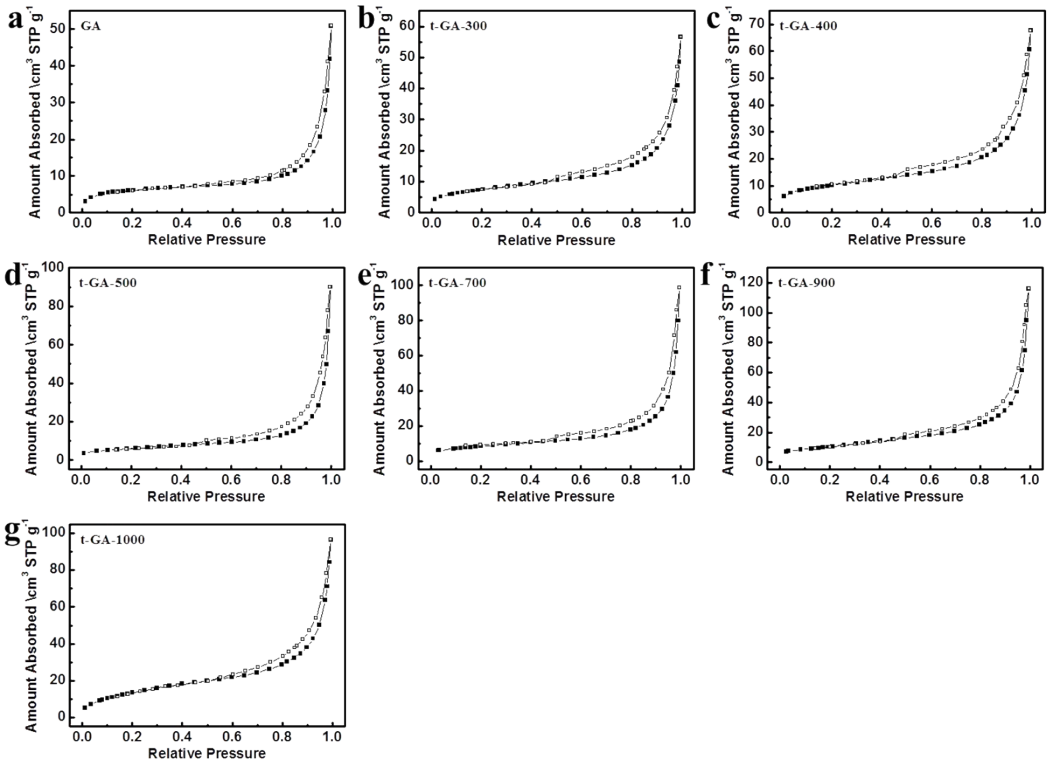

Figure S18. N_2 adsorption-desorption isotherms of GA (a), t-GA-300 (b), t-GA-400 (c), t-GA-500 (d), t-GA-700 (e), t-GA-900 (f), and t-GA-1000 (g).

The Porosity Data of GA and t-GA-(300~1000)

Table S6. Specific surface area, pore size, and pore volume of the GA and t-GA-(300~1000).

Sample	Specific surface area [$m^2\ g^{-1}$]	Pore size [nm]	Pore volume [$cm^3\ g^{-1}$]
GA	22.1	7.8	0.07
t-GA-300	26.2	8.2	0.09
t-GA-400	36.4	7.7	0.10
t-GA-500	31.5	11.4	0.14
t-GA-700	30.9	10.3	0.15
t-GA-900	37.6	10.1	0.18
t-GA-1000	32.2	9.3	0.12

Schematic Illustration of the GA before and after Compression

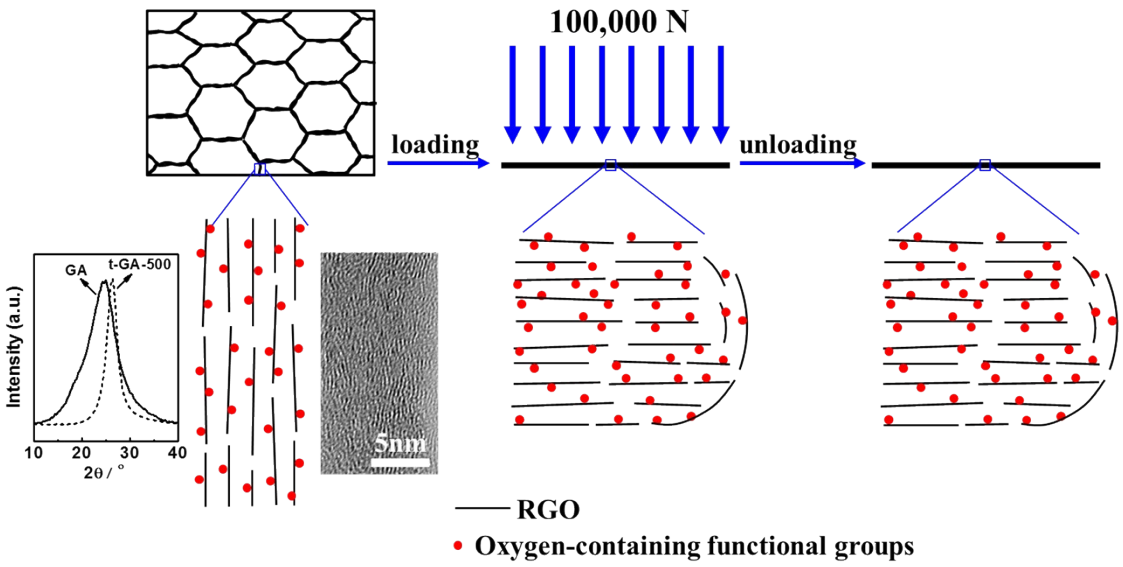

Figure S19. Schematic illustration of the GA inside deformation during the ultimate compress/release cycle. Insert: the XRD pattern and HRTEM image for the GA (the XRD pattern for t-GA-500: dashed line).

Methods

1. Materials

Graphite powder was obtained from Qingdao Henglide Graphite Co., Ltd. (China). Acrylamide (AAm) and potassium peroxydisulfate (KPS) were provided by Xilong Chemical Co., Ltd. (China). Methylene-bis-acrylamide (MBAA), and ascorbic acid were purchased from Sinopharm Chemical Reagent Co., Ltd. (China). $KMnO_4$, concentrated H_2SO_4 (98%), concentrated hydrochloric acid (36-38%), and hydrogen peroxide (30%) were purchased from Beijing Chemical Factory (China). A dialysis bag (molecular-weight cut off of 14,000) was purchased from Beijing Jingke Hongda Biotechnology Co., Ltd. (China).

2. Sample Preparation

Preparation of GO

GO was synthesized from natural graphite powder using a modified Hummers' method.[S16] The graphite powder (10 g) was added to an 80 °C solution of concentrated H_2SO_4 (60 mL), $K_2S_2O_8$ (5 g), and P_2O_5 (5 g). The resulting dark-blue mixture was thermally isolated and allowed to cool to room temperature over a period of 6 h. The mixture was then carefully diluted with distilled water, filtered, and washed on the filter until the pH of the rinsing water became neutral. The product was dried in air at the ambient temperature overnight. This pre-oxidized graphite was then subjected to oxidation by Hummers' method. The oxidized graphite powder (10 g) was placed into the cold (0 °C) concentrated H_2SO_4 (460 mL). $KMnO_4$ (30 g) was added gradually with stirring and cooling so that the temperature of the mixture never exceeded 20 °C. The mixture was then stirred at 35 °C for 2 h, and distilled water (460 mL) was added. After 15 min, the reaction was terminated by the addition of a large amount of distilled water (1.4 L) and a 30% H_2O_2 solution (25 mL), after which the color of the mixture changed to bright yellow. The mixture was filtered and washed with a 1:10 HCl solution (2.5 L) in order to remove the metal ions. The GO product was suspended in distilled water to form a viscous, brown dispersion, which was subjected to dialysis to completely remove the metal ions and acids. The concentration of the GO solution was adjusted to 2~10 mg mL^{-1} before it was treated by ultrasonication for 2 h for further experiments.

Physical Characterizations

1. Atomic Force Microscope (AFM)

Atomic force microscopy (AFM) images were recorded under ambient conditions using a Digital Instrument Multimode Nanoscope IIIA operating at a tapping mode. Samples were

prepared by spin-coating a dispersion of GO in water (0.3 mg mL^{-1}) onto a freshly cleaved mica surface. The average size of the GO sheets is less than 5 μm and the height difference between the steps is ~0.8 nm (**Figure S1**), representing the typical height of an individual GO sheet.

2. Scanning Electron Microscopy (SEM)

SEM images were obtained on a field-emission scanning electron microscope (S4800, Hitachi, Japan) using an accelerating voltage of 10 kV (**Figures 1b**, **3a**, **5**; **Figures S3** and **S10-S12**). All samples were spray-coated with a thin gold layer in vacuum prior to the SEM observations.

3. Transmission Electron Microscopy (TEM)

High-resolution transmission electron microscopy (HRTEM) images were obtained using TEM instruments (JEM-2100, JEOL, Japan) operated at an accelerating voltage of 200 kV (**Figures 1c** and **6; Figures S10** and **S19**).

For observing the cell walls of graphene aerogels, a piece of graphene aerogel was scraped by copper grid for three times and the TEM and HRTEM analysis were taken.

4. X-Ray Diffraction (XRD)

X-ray diffraction (XRD) patterns were recorded using a Rigaku D/MAX-RB diffractometer (40 kV, 30 mA) with Cu-Kα radiation with a scanning rate of 3 ° min^{-1} for 2 θ from 10 ° to 40 ° (**Figures 1d**, **4c**, **6**; **Figure S19**).

5. X-ray Photoelectron Spectroscopy (XPS)

X-ray photoelectron spectroscopy (XPS) measurements were carried out with an ESCALab220i-XL photoelectron spectrometer from VG Scientific (**Figure 1e**; **Figure S17**; **Table S5**).

6. Thermal Gravimetric Analysis (TGA)

Thermal gravimetric analysis (TGA) was carried out using a thermogravimetric analyzer (Pyris 1, PerkinElmer, USA) from 50 to 700 °C at a heating rate of 10 °C min^{-1} under a N_2 atmosphere (**Figure 1g**). The sample was heated from 50 to 1000 °C at a heating rate of 10 °C min^{-1} under a N_2 atmosphere and annealed at 300, 400, 500, 700, 900, and 1000 °C for 1h, respectively (**Figure S14**). Before the measurements, all samples were dried in vacuum at 50 °C for 12 h.

7. Measurements of Nitrogen Sorption

Nitrogen sorption measurements were performed with a Micromeritics TriStar II 3020 ASAP (Micromeritics, USA) to obtain pore properties such as the BET-specific surface area, pore size distribution, and total pore volume (**Figure S18** and **Table S6**). Before measurement, the sample was outgassed under vacuum at 100 °C for 10 h until the pressure less than 0.665 Pa.

8. Compression Testing

The compressive tests (90% strain) were performed with a rheometer (ARES-G2, TA Instruments, USA) using a 20 N load cell in the axial-compression testing mode at a strain rate of 10 mm min^{-1}. The cyclic compressions were conducted at room temperature (**Figures 2a-c**; **Figures S6**, **S7**, and **S16**; **Table S1**; **Movies S1** and **S2**). The compression tests were performed under different temperatures (low temperature (-150 °C in N_2), room temperature (20 °C), and high temperature (450 °C in N_2), respectively) (**Figure 2d**).

The compressive tests (above 99% strain) were performed in an Instron (3365, Instron, USA) using a 5000 N load cell in the axial-compression testing mode at a strain rate of 10 mm min^{-1} (**Figures 2e-f** and **Figures 3b-g**; **Tables S3** and **S4**; **Movie S3**) and different strain rate (1 mm~300 mm min^{-1}) (**Figure S9**).

The compressive tests (above 99.8% strain) were performed in a mould pressing machine (FM450, Beijing Future Material Sci-tech Co., Ltd, China) under 100,000 N for 60 min (**Figure 3**; **Tables S3** and **S4**). Here, we choose the lead-tin alloy with good ductility and deformability to measure the thickness of t-GA-500 during compression test. As shown in **Figure S13**, t-GA-500 (height: 1.3 cm, diameter: 1.2 cm) and three little pellets (diameter: ~0.5 mm) of lead-tin alloy were put around the t-GA-500 on the cylindrical molds (height: 0.5 cm, diameter: 6.0 cm) and the molds were compressed under 100,000 N for 60 min. After compression, t-GA-500 recover into its original shape and the lead-tin alloy little pellets became thin foils. We could get the thickness of t-GA-500 during the compression according to the average thickness of lead-tin alloy foils. The thicknesses and maximum strains of t-GA-500 during the extreme compression (100,000 N, 60 min) are listed in **Table S2**. And the ultimate stress of t-GA-500 during the compression (100,000 N) is calculated by the loading and cross-sectional area of sample and are listed in **Tables S3** and **S4**.

9. Measurements of Electrical-Conductivity

The electrical conductivity of samples were measured by a two-point probe (Keithley 2000, Keithley, USA) at room temperature (**Figures 4e-f**). To optimize the electrical contact between the copper wires and the sample, both ends of the sample were carefully coated with a thin layer of silver paste.

Supporting References

[S1] L. Qiu, Z. Liu, L. Y. Chang, Y. Z. Wu, D. Li. Biomimetic superelastic graphene-based cellular monoliths. *Nat. Commun.* **2012**, *3*, 1241.

[S2] C. W. Li, L. Qiu, B. Q. Zhang, D. Li, C. Y. Liu. Robust vacuume/air dired graphene aerogels and fast recoverable shape-memory hybrid foams. *Adv. Mater*. **2016**, *28*, 1510.

[S3] J. Zhong, J. Meng, X. C. Gui, T. Hu, N. Xie, X. Y. Lu, Z. Y. Yang, N. Koratkar. Nanocarbon aerogel complexes inspired by the leaf structure. *Carbon* **2014**, *77*, 637.

[S4] X. Wang, L. L. Lu, Z. L. Yu, X. W. Xu, Y. R. Zheng, S. H. Yu. Scalable template synthesis of resorcinol-formaldehyde/graphene oxide composite aerogels with tunable densities and mechanical properties. *Angew. Chem. Int. Ed*. **2015**, *127*, 2427.

[S5] H. W. Liang, Q. F. Guan, L. F. Chen, Z. Zhu, W. J. Zhang, Y. S. Hong. Macroscopic-scale template synthesis of robust carbonaceous nanofiber hydrogels and aerogels and their applications. *Angew. Chem. Int. Ed.* **2012**, *51*, 5101.

[S6] N. Ni, S. Barg, E. G. Tunon, F. M. Perez, M. Miranda, C. Lu, C. Mattevi, E. Saiz. Understanding mechanical response of elastomeric graphene networks. *Sci. Rep*. **2015**, *5*, 13712.

[S7] K. H. Kim, Y. Oh, M. F. Islam. Graphene coating makes carbon nanotube aerogels superelastic and resistant to fatigue. *Nat. Nanotechnol*. **2012**, *7*, 562.

[S8] Z. Y. Wang, X. Shen, M. A. Garakani, X. Y. Lin, Y. Wu, X. Liu, X. Y. Sun, J.-K. Kim. Graphene aerogel/epoxy composites with exceptional anisotropic structure and properties. *ACS Appl. Mater. Interfaces* **2015**, *7*, 5538.

[S9] H. Hu, Z. B. Zhao, W. B. Wan, Y. Gogotsi, J. S. Qiu. Ultralight and highly compressible graphene aerogels. *Adv. Mater.* **2013**, *25*, 2219.

[S10] H. L. Gao, Y. B. Zhu, L. B. Mao, F. C. Wang, X. S. Luo, Y. Y. Liu, Y. Lu, Z. Pan, J. Ge, W. Shen, Y. R. Zheng, L. Xu, L. J. Wang, W. H. Xu, H. A. Wu, S. H. Yu. Super-elastic and fatigue resistant carbon material with lamellar multi-arch microstructure. *Nat. Commun.* **2016**, *7*, 12920.

[S11] J. Kuang, Z. H. Dai, L. Q. Liu, Z. Yang, M. Jin, Z. Zhang. Synergistic effects from graphene and carbon nanotubes endow ordered hierarchical structure foams with a combination of compressibility, super-elasticity and stability and potential application as pressure sensors. *Nanoscale* **2015**, *7*, 9252.

[S12] X. Xu, H. Li, Q. Q. Zhang, H. Hu, Z. B. Zhao, J. H. Li, J. Y. Li, Y. Qiao, Y. Gogotsi. Self-sensing, ultralight, and conductive 3D graphene/iron oxide aerogel elastomer deformable in a magnetic field. *ACS Nano* **2015**, *9*, 3969.

[S13] Q. Q. Zhang, X. Xu, H. Li, G. P. Xiong, H. Hu, T. S. Fisher. Mechanically robust honeycomb graphene aerogel multifunctional polymer composites. *Carbon* **2015**, *93*, 659.

[S14] H. Bi, I. W. Chen, T. Q. Lin, F. Q. Huang. A new tubular graphene form of a tetrahedrally connected cellular structure. *Adv. Mater.* **2015**, *27*, 5943.

[S15] Y. P. Wu, N. B. Yi, L. Huang, T. F. Zhang, S. L. Fang, H. C. Chang, N. Li, J. Y. Oh, J. A. Lee, M, Kozlov, A. C. Chipara, H. Terrones, P. S. Xiao, G. K. Long, Y. Huang, F. Zhang, L. Zhang, X. Lepró, C. Haines, M. D. Lima, N. P. Lopez, L. P. Rajukumar, A. L. Elias, S. M.

Feng, S. J. Kim, N. T. Narayanan, P. M. Ajayan, M. Terrones, A. Aliev, P. F. Chu, Z. Zhang, R. H. Baughman, Y. S. Chen. Three-dimensionally bonded spongy graphene material with super compressive elasticity and near-zero Poisson's ratio. *Nat. Commun.* **2015**, *6*, 6141.

[S16] Q. Q. Zhang , X. Xu , D. Lin , W. L. Chen, G. P. Xiong, Y. K. Yu, T. S. Fisher, H. Li. Hyperbolically patterned 3D graphene metamaterial with negative poisson's ratio and superelasticity. *Adv. Mater.* **2016**, *28*, 2229.

[S17] X. Xu, Q. Q. Zhang, Y. K. Yu, W. L. Chen, H. Hu, H. Li. Naturally dried graphene aerogels with superelasticity and tunable poisson's ratio. *Adv. Mater.* **2016**, *28*, 9223.

[S18] L. X. Lv, P. P. Zhang, H. H. Cheng, Y. Zhao , Z. P. Zhang ,G. Q. Shi, L. T. Qu. Solution-processed ultraelastic and strong air-bubbled graphene foams. *Small* **2016**, *12*, 24, 3229.

[S19] Z. Wang, Z. Dai, J. J. Wu, N. Zhao, J. Xu. Vacuum-Dried Robust Bridged Silsesquioxane Aerogels. *Adv. Mater.* **2013**, *25*, 4494.

[S20] S. O. Kucheyev, M. Stadermann, S. J. Shin, J. H. Satcher Jr., S. A. Gammon, S. A. Letts, T. van Buuren, A. V. Hamza, Super-Compressibility of Ultralow-Density Nanoporous Silica. *Adv. Mater.* **2012**, *24*, 776.

[S21] L. Mu, S. D. Yang, B. Hao, P. C. Ma, Ternary Silicone Sponge with Enhanced Mechanical Properties for Oil-water Separation. *Polym. Chem.*, **2015**, *6*, 5869.

[S22] T. A. Schaedler, A. J. Jacobsen, A. Torrents, A. E. Sorensen, J. Lian, J. R. Greer, L. Valdevit, W. B. Carter, Ultralight Metallic Microlattices. *Science* **2011**, *334*, 962.

[S23] X. Y. Zheng, H. Lee, T. H. Weisgraber, M. Shusteff, J. DeOtte, E. B. Duoss, J. D. Kuntz, M. M. Biener, Q. Ge, J. A. Jackson, S. O. Kucheyev, N. X. Fang, C. M. Spadaccini, Ultralight, Ultrastiff Mechanical Metamaterials. *Science* **2014**, *344*, 1373.

[S24] L. R. Meza, S. Das, J. R. Greer, Strong, Lightweight, and Recoverable Three-Dimensional Ceramic Nanolattices. *Science* **2014**, *345*, 1322.

[S25] T. L. Zhai, Q. F. Zheng, Z. Y. Cai, L. S. Turng, H. S. Xia, S. Q. Gong, Poly(vinyl alcohol)/Cellulose Nanofibril Hybrid Aerogels with an Aligned Microtubular Porous Structure and Their Composites with Polydimethylsiloxane. *ACS Appl. Mater. Interfaces* **2015**, *7*, 7436.

[S26] H. L. Gao, Y. Lu, L. B. Mao, D. An, L. Xu, J. T. Gu, F. Long, S. H. Yu, A Shape-Memory Scaffold for Macroscale Assembly of Functional Nanoscale Building Blocks. *Mater. Horiz.*, **2014**, *1*, 69.

[S27] H. Z. Sai, R. Fu, L. Xing, J. H. Xiang, Z. Y. Li, F. Li, T. Zhang, Surface Modification of Bacterial Cellulose Aerogels' Web-like Skeleton for Oil/Water Separation. *ACS Appl. Mater. Interfaces* **2015**, *7*, 7373.

[S28] S. B. Ye, J. C. Feng, P. Y. Wu, Highly Elastic Graphene Oxide-Epoxy Composite Aerogels via Simple Freeze-drying and Subsequent Routine Curing. *J. Mater. Chem. A*, **2013**, *1*, 3495.

[S29] H. Lu, C. W. Li, B. Q. Zhang, X. Qiao, C. Y. Liu, Toward Highly Compressible Graphene Aerogels of Enhanced Mechanical Performance with Polymer. *RSC Adv.*, **2016**, *6*, 43007.

[S30] J. Ge, L. A. Shi, Y. C. Wang, H. Y. Zhao, H. B. Yao, Y. B. Zhu, Y. Zhang, H. W. Zhu, H. A. Wu, S. H. Yu, Joule-heated Graphene-Wrapped Sponge Enables Fast Clean-up of Viscous Crude-Oil Spill, *Nat. Nanotechnol*. **2017**, *12*, 434.

[S31] C. Wu, X. Y. Huang, X. F. Wu, R. Qian, P. K. Jiang, Mechanically Flexible and Multifunctional Polymer-Based Graphene Foams for Elastic Conductors and Oil-Water Separators. *Adv. Mater.* **2013**, *25*, 5658.

[S32] Q. Y. Peng, Y. B. Li, X. D. He, X. C. Gui, Y. Y. Shang, C. H. Wang, C. Wang, W. Q. Zhao, S. Y. Du, E. Z. Shi, P. X. Li, D. H. Wu, A. Y. Cao, Graphene Nanoribbon Aerogels Unzipped from Carbon Nanotube Sponges. *Adv. Mater.* **2014**, *26*, 3241.

[S33] X. S. Du, H. Y. Liu, Y. W. Mai, Ultrafast Synthesis of Multifunctional N-Doped Graphene Foam in an Ethanol Flame. *ACS Nano* **2016**, *10*, 453.

[S34] C. W. Li, D. G. Jiang, H. Liang, B. B. Huo, C. Y. Liu, W. R. Yang, J. Q. Liu, Superelastic and Arbitrary-Shaped Graphene Aerogels with Sacrifcial Skeleton of Melamine Foam for Varied Applications. *Adv. Funct. Mater.* DOI: 10.1002/adfm.201704674.

[S35] Y. A. Samad, Y. Q. Li, A. Schiffer, S. M. Alhassan, K. Liao, Graphene Foam Developed with a Novel Two-Step Technique for Low and High Strains and Pressure Sensing Applications. *Small* **2015**, *11*, 2380.

[S36] D. G. Jiang, C. W. Li, W. R. Yang, J. Z. Zhang, J. Q. Liu, Fabrication of an Arbitrary-Shaped and Nitrogen-Doped Graphene Aerogel for Highly Compressible all Solid-State Supercapacitors. *J. Mater. Chem. A*, **2017**, *5*, 18684.

[S37] Y. A. Samad, Y. Q. Li, S. M. Alhassan, K. Liao, Novel Graphene Foam Composite with Adjustable Sensitivity for Sensor Applications. *ACS Appl. Mater. Interfaces* **2015**, *7*, 9195.